Iraqi Journal of Scientific and Industrial Research
Volume 1, Issue (2), April-June 2022, pp. 42-49

Atomic and Electronic Structures of NiO/Gold Interfaces Fabricated by Medium Energy Ion Scattering

Fadhil A. HASAN

Department of Physics, College of Science, University of Kufa, Al-Najaf Province, IRAQ

Abstract

The atomic and electronic structures of NiO(001)/Au(001) interfaces were analyzed by high-resolution medium energy ion scattering (MEIS) and photoelectron spectroscopy using synchrotron-radiation-light. The MEIS analysis clearly showed that O atoms were located above Au atoms at the interface and the inter-planar distance of NiO(001)/Au(001) was derived to be 2.30±0.05Å, which were consistent with the calculations based on the density functional theory (DFT). We measured the valence band spectra and found metallic features for the NiO thickness up to 3 monolayer (ML). Relevant to the metallic features, electron energy loss analysis revealed that the band gap for NiO(001)/Au(001) reduced with decreasing the NiO thickness from 10 down to 5 ML. We also observed Au 4f lines consisting of surface, bulk, and interface components and found a significant electronic charge transfer from Au(001) to NiO(001). The present DFT calculations demonstrated the presence of an image charge beneath Ni atoms at the interface just like alkali-halide/metal interface, which may be a key issue to explain the core level shift and band structure.

Keywords: Thin films; Interfaces; MEIS; Photoelectron spectroscopy

Received: 2 August 2021; **Revised:** 3 October 2021; **Accepted:** 10 October 2021; **Published:** 1 January 2022

1. Introduction

The electronic contact between metal and oxide is an important issue in terms of oxide electronics, which has recently attracted much attention [1-3]. It has been also revealed that electronic charge transfers between metal and oxide supports play a crucial role in catalytic activities, in particular, for Au nano-particles on oxide supports [4-6]. NiO is one of the most frequently utilized oxide supports as catalyst. Indeed, Au nano-particles grown on NiO supports work well as catalyst in CO oxidation and other reactions [7,8]. Aside from such applications, NiO is known as a typical anti-ferromagnetic and charge transfer type insulating material [9,10]. The mechanism for emerging large band gap of 4.3 eV is still a debatable issue. Much attention has been also paid to the electronic and magnetic properties of the ultra-thin films dependent on the thickness and substrate materials [11-14]. In the latter case, an electronic charge transfer which induces an interface dipole plays a crucial role [15].

There are many reports on the interface structure of NiO(001)/Ag(001), which were analyzed by tensor low energy electron diffraction (LEED) analysis [16,17] and by extended X-ray absorption fine structure (EXAFS) technique [12,18]. A similar structure is expected for NiO(001)/Au(001) but not analyzed experimentally so far. Concerning Au deposition on NiO(001) substrates, it was reported that the Au grew initially in a two-dimensional (2D) mode and then took a form of 3D islands [19-21] and a remarkable chemical reduction of the NiO occurred at the interface [19,21]. It must be, here, noted that the growth mode for NiO thin layers on Au(001) substrate is different from that for Au on NiO(001), which will be mentioned later. As well known, the polar NiO(111) surface is energetically unstable and thus the surface grown on Au(111) takes a reconstructed octopolar structure [22,23]. There is also no report on the interface structure of the NiO(111)/Au(111).

In this study, we formed epitaxially ultra-thin NiO(001) layers on Au(001) thin films, which were also epitaxially grown on Ag(001) substrate. Then the atomic and electronic interface structures were analyzed by high-resolution medium energy ion

© All Rights Reserved

scattering (MEIS) combined with photoelectron spectroscopy using synchrotron-radiation (SR) light [24]. First we determined using MEIS the inter-layer distance of the NiO(001)/Au(001) and which atomic species was located above the Au atoms at the interface. Then observations of valence band as well as Au 4f core level spectra were carried out using polarized SR light. Inelastic electron energy loss spectra were also measured to determine the band gap of the NiO(001) stacked on the Au(001) films dependent on the NiO thickness. The results obtained were discussed in detail considering the *ab initio* calculations by VASP (Vienna *ab initio* simulation package) [25,26] using the Dudarev' approach to treat on-site Coulomb interaction in NiO [27].

2. Experimental Part

We prepared a clean (1×1) surface of Ag(001) substrate by repeating Ar^+-sputtering/annealing cycle and finished by annealing at 550°C for 30 min UHV. Then an Au(001) thin film with thickness of ~10 atomic layer was epitaxially grown at RT on the Ag(001) substrate at a deposition rate of 0.35 ML/min. Finally, NiO(001) thin layers were grown epitaxially on the Au(001) at a rate of 0.39 Ag(001)-(1x1) ML/min in O_2 atmosphere (1×10^{-6} Torr) at room temperature (RT). The thickness ranged from 1 up to 10 mono-layer (ML: 1 ML = 2.30×10^{15} atoms/cm^2 10^{15}: areal density of NiO(001), 1.20×10^{15} atoms/cm^2 for Au(001)) and the crystalline quality was checked by reflection high energy diffraction (RHEED). Note that the lattice mismatch between Au and Ag is 0.2 % and that between Au and NiO is 2.2 % (lattice constant: 4.079 Å for Au and 4.17 Å for NiO at RT). It is essential to grow NiO(001) layers on thin Au(001) films in order to avoid overlapping the scattering signals from Ni and deep Au layers in MEIS spectra. Figure (1) shows the RHEED patterns observed at [110]-azimuth for Ag(001), Au(001) (~10ML)/Ag(001), and NiO(001) (2ML)/Au(001) (~10ML)/Ag(001), from the top to bottom. The (20×5) reconstructed structure [28] was seen for the Au(001) clean surface. After NiO (2ML) deposition, the long range ordered structure disappeared and broad NiO(001) lines emerged. It has to be noted that previous studies carried out on NiO(001)/Ag(001), the system which is supposed to resemble to NiO/Au, showed that NiO layers covered the Ag surface completely at the coverage of 2 ML [16]. Smaller coverages result in incomplete surface occupancy. For this reason the main structural analysis in the present work was carried out for 2ML NiO coverage, although electronic properties of the valence band including band gap were analyzed in a wide range of NiO thickness from 1 up to 10 ML.

The samples were then transferred to MEIS and photoemission chambers maintaining ultra-high vacuum (UHV) conditions. Monochromated SR photons were incident on the sample surface and emitted photoelectrons were detected by a concentric hemispherical electrostatic analyzer (ESA) under normal emission condition. The incident photon energy was calibrated using the second harmonic waves by measuring bulk Au $4f_{5/2}$, $_{7/2}$ lines and the position of the Fermi level was assigned as the Fermi edge measured for a poly-crystal Au film. We determined the work function of the hemispherical ESA assuming the binding energy of Au $4f_{7/2}$ to be E_B=84.0 eV (bulk component). The photoemission chamber was equipped with an electron gun, which allowed for observing electron inelastic energy loss spectra providing the values of the band gap of NiO(001). The photoemission and MEIS analyses together with the sample preparation were performed *in situ* under UHV condition ($\leq2\times10^{-10}$ Torr) throughout the experiments.

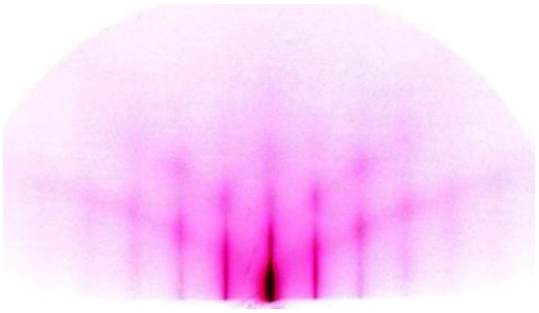

(a) Ag(001)-(1x1)

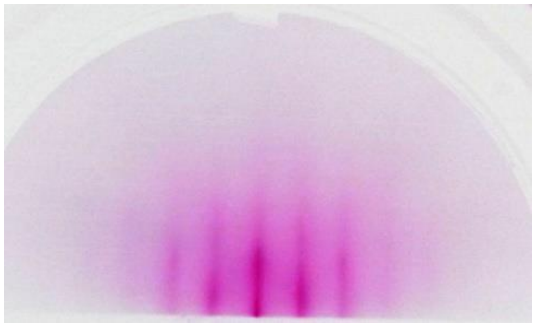

(b) 10M Au(001)-(20x5)/Ag(001)

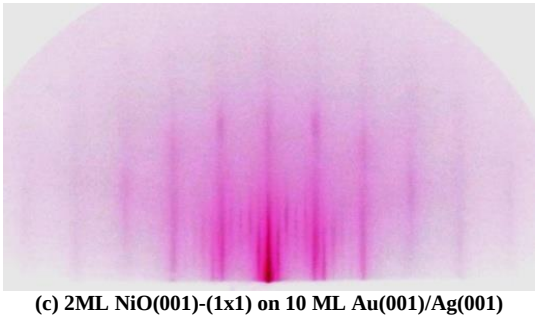

(c) 2ML NiO(001)-(1x1) on 10 ML Au(001)/Ag(001)

Fig. (1) RHEED patterns observed for Ag(111), 10 ML-Au(001)/Ag(001), and 2 ML-NiO(001)/10 ML-Au(001)/Ag(001) from the top to bottom

© All Rights Reserved

High-resolution MEIS using 80 and 120 keV He^+ ions made it possible to identify which atom, O or Ni is located on top of Au atom at the NiO(001)/Au(001) interface and also to determine the inter-planar distance between NiO(001) and Au(001) using the shadowing and blocking effects. To do that, we performed Monte Carlo (MC) simulations of He^+ ion trajectories assuming the interface atomic structure to reproduce the observed MEIS spectra. The scattering yield from atomic species *j* in *n*-th layer is given by

$$Y_j(n) = Q\,(d\sigma_j/d\Omega)\cdot\Delta\Omega\cdot c_j^{(n)}\cdot P_{CL}^{(j)}(n)\cdot\varepsilon\,\eta_+/\cos\theta_{in} \quad (1)$$

where Q, $d\sigma_j/d\Omega$, $\Delta\Omega$, $c_j^{(n)}$, ε and θ_{in} respectively are number of incident He^+ ions, differential scattering cross section calculated from Molière potential, solid angle subtended by the detector, number of atomic species *j* in the *n*-th layer, detection efficiency of the position sensitive detector (0.44 as measured previously), and incident angle with respect to surface normal. Here, η_+ is He^+ fraction dependent on the surface material and emerging energy of He^+ ions and $P_{CL}^{(j)}(n)$ is the close encounter ions and *PCL* probability for the atom *j* in the *n*-th layer, which was calculated by the MC simulations of He ion trajectories. The η_+ value for He ions scattered from Au were measured in advance employing thin Au films deposited on Ni(111) whose thickness was determined by Rutherford backscattering using 2.0 MeV He^+ ions and that for NiO surface was estimated from the data obtained for rutile TiO_2(110) whose surface structure was already known.

3. Results and Discussion

We first determine which atomic species, O or Ni atom is located above the Au atom at the NiO/Au interface by means of high-resolution MEIS. Figure (2) shows the MEIS spectrum observed for 80 keV He^+ ions incident along the [110]-axis of NiO(5ML)/Au(001)-(~10ML)/Ag(001) and scattered to the [110] direction. Unexpectedly we observed a broad and intense Au surface peak, which is probably due to formation of Au clusters and partly due to tetragonal distortion of the overlying NiO(001) film[18].

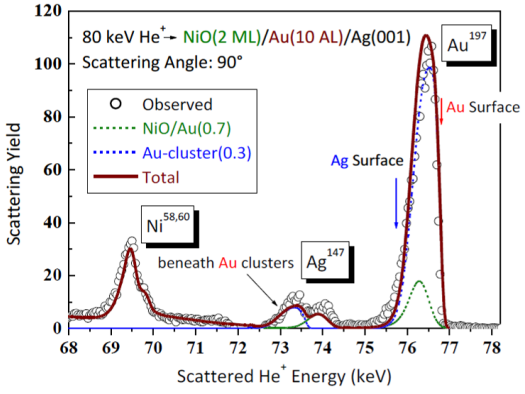

Fig. (2) MEIS spectrum (circles) observed for 80 keV He^+ ions incident on NiO(2ML)/Au(10ML)/Ag(001) at 45° and scattered to 45° with respect to surface normal at [100]-azimuth of Ag(001). Thin solid curves denote simulated spectra from the regions covered with NiO (70%) and with Au clusters (30%). Thick solid curve corresponds to simulated total MEIS spectrum. Vertical arrows indicate the energy position for He^+ ions scattered from Au and Ag atom on top of the surface

Indeed, the observed MEIS spectrum was reproduced well by assuming Au clusters on the NiO(001) surface with average diameter and height of 3.0 and 0.85 nm, respectively and areal occupation of 30%. This indicates that Au atoms were segregated on the NiO(001) surface to form thin islands (total amount of Au islands: 4.3×10^{14} atoms/cm^2 corresponds to ~0.35ML). The small peak (decomposed) from Au beneath NiO(001) is attributed to the double alignment geometry ([101]-incidence and [101]-emergence: strong shadowing effect), while the large contribution from Au clusters indicates their random orientation in the lateral direction. The double peak coming from Ag corresponds to scattering components from Ag beneath NiO (70%) and Au clusters (30%). Note that the probing depth of the present MEIS analysis is 5-10 nm maintaining a good depth resolution. The reason why the intensity ratio of the double peak does not correlate with the areal occupation ratio cannot be explained clearly. The randomly oriented Au clusters in the lateral direction may increase the dechanneling fraction, which enhances the scattering yield from the underlying Ag atoms.

Then we fixed the incident direction ~3° off from the [101]-axis (random incidence) and scanned the emerging angle at the [100]-azimuth from 10 to 65° with respect to surface normal (see Fig. 3a). Figure (3b) shows the observed angular scan spectrum for NiO (2ML)/Au(001)-(~10ML)/Ag(001) and simulated spectra assuming O atom above Au atom (blue solid curve) and Ni above Au (red dashed curve). In the MC simulations of He^+ ion trajectories, it was assumed that the root mean square (r.m.s.) thermal vibration amplitudes (one dimensional) for Ni and O are 0.08Å (same) [29] and 0.088Å for Au derived from Debye temperature (180K). Also assume the vibrations in the surface normal direction are enhanced by 2 compared with that for bulk. The scattering yield from all the Au atoms is plotted as a function of emerging angle. Here, we assumed the interlayer distance of 2.45Å at the NiO(001)/Au(001)-(10ML) interface, which was reported previously for NiO(001)/Ag(001) [16]. It is clearly seen that there exist a large dip around 43°, whereas no angular dip around 25°, indicating O atoms located above Au at the NiO(001)/Au(001) interface. After background subtraction, the observed angular scan spectrum was well reproduced assuming the surface consisting of NiO(001) (70%) and Au clusters (30%) and the

© All Rights Reserved

interlayer distance of 2.30±0.05 Å, as shown in Fig. (3c). As previous studies showed, in the case of NiO(001)/Ag(001), it was revealed that the O atoms are located on top of Ag atoms and the Ni-Ag distance is 2.43±0.05Å determined by tensor low energy electron diffraction (LEED) analysis [16] and 2.3±0.1Å and 2.37±0.05Å, respectively obtained by primary beam diffraction modulated electron emission (PDMEE) and by polarization-dependent x-ray absorption spectroscopy (XAS) [12]. Considering the similar electronic properties of Au and Ag and good lattice matching between them, the above MEIS result seems quite adequate. It was also evidenced that the Ag(001) surface was covered completely with NiO(001) for coverages above 2ML of NiO by Ni deposition at RT under O_2 atmosphere [16].

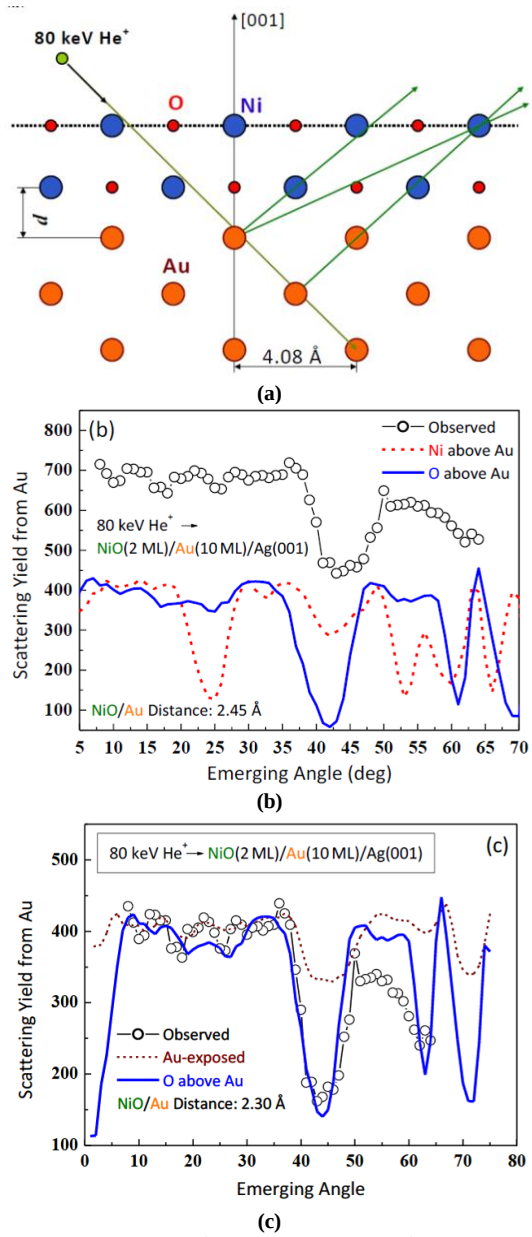

Fig. (3) (a) Side view of scattering geometry for 80 keV He+ ions incident at a fixed random direction on NiO(001)-2ML/Au(001)-10 ML/Ag(001) at [100]-azimuth. Blue, red and orange circles denote Ni, O and Au atoms, respectively, (b) Observed angular scan spectrum (circles) for scattering component from Au as a function of emerging angle scaled from surface normal. Thick solid and dashed curves, respectively are simulated angular scan profiles assuming O atoms above Au and Ni atoms above Au at the interface. Pseudomorphic NiO(001) layer stacking on Au(001) and the interlayer distance of 2.45Å were assumed, and (c) Observed angular scan spectrum after subtracting background level to match the simulated one at emergence in random directions. Thick solid curve is simulated spectrum assuming the surface covered with NiO (70%) and Au-clusters (30%) and the interlayer distance of 2.30Å. Dashed curve indicates the simulated angular scan spectrum for all surface covered with Au clusters

According to the recent report [30], atomic oxygen exposure allowed control at the atomic scale of chemical and structural interface of NiO(001)/Ag(001). This technique can probably give a good quality of the NiO(001)/Au(001) interface. Observed RHEED patterns, however, clearly showed epitaxial NiO(001) layers on the Au(001) films and the valence band spectrum for 3ML NiO(001) stacked on Au(001) became close to that for bulk NiO(001). Therefore, the analysis using the present sample gives enough meaningful information. Next, we observed the valence band spectra at photon energy of 130 eV for Au(001)(~10ML)/Ag(001) before and after NiO(1-3ML) deposition as well as Ni(111) and NiO(001) single crystal substrates, which is shown in Fig. (4). Note that single crystal NiO(001) spectrum was recorded using p-type semiconducting NiO substrate obtained by annealing in UHV to avoid charge-up. In addition to Au $5d_{3/2}$ and $5d_{5/2}$ lines, a strong Ni 3d peak with metallic feature appeared at ~1 eV below the Fermi level (E_F) for NiO(001)(1ML)/Au(001). According to Caffio et al. [16], there coexist Ni and NiO islands at 1ML NiO deposition and complete NiO(001) coverage was achieved after 2ML NiO deposition on Ag(001) substrate. After stacking of 2ML of NiO(001), the Ni 3d peak with metallic property shifted slightly to higher binding energy side and the satellite line from NiO appeared at E≅10 eV [31]. The Ni 3d peak coincides with that coming from bulk NiO (main line: $3d^8$ L^{-1} configuration; L: O^{2-}) and the satellite line ($3d^7$ L) clearly emerged. Interestingly, the 3 ML-NiO(001) stacked on Au(001) has still a metallic feature. This is consistent with the theoretical prediction that the NiO/Ag(001) interfacial layer is metallized even for 5-ML NiO stacking [32]. It must be noted that the contribution from Au 6s band is small enough not to disturb the apparent spectrum near the Fermi edge because of its delocalized nature and a small occupancy (~1 electron) (see the valence band spectrum for Au(001) surface in Fig. 4).

© All Rights Reserved

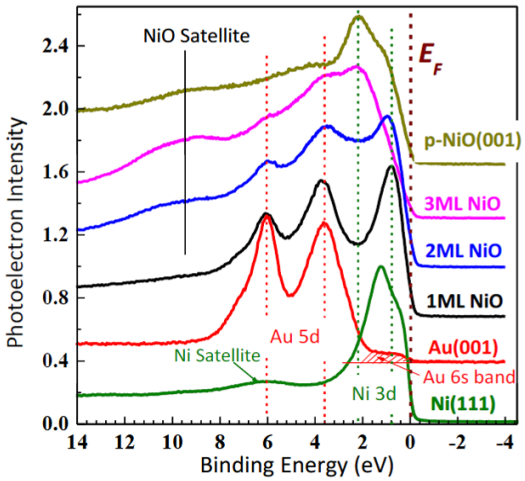

Fig. (4) Valence band spectra observed at 130 eV photon incidence for Ni(111), Au(001), NiO(1ML)/Au(10 ML), NiO(2 ML)/Au(10 ML), NiO(3 ML)/Au(10 ML), and p-type NiO(001) crystal from bottom to top. The cross-hatched area for Au(001) surface indicates Au 6s band. Photoelectrons emitted to surface normal direction were detected with hemispherical electrostatic analyzer

We then observed Au 4f core level for Au(001)-(5×20) surface and onto which 1, 2, and 3 ML NiO(001) layers were grown epitaxially. Figure (5) shows the spectra measured at incident photon energy of 130 eV under normal emission condition. For clean Au(001)-(5×20) surface, the spectrum consists of two components; bulk and surface. The Au $4f_{7/2}$ line appeared at 83.62 and 84.0 eV, which were identified as the surface and bulk component, respectively [33,34]. Here, we employed the Doniach-Sunjic line shape [31] with an asymmetric parameter α=0.06 and full width at half maximum: FWHM = 0.32eV, according to Hsieh et al. [33]. After NiO(001) deposition, the Au 4f line shifted to higher *EB* side with increasing NiO thickness. This is due to decrease in the intensity of the surface component and to increase in the intensity of the interface component, which appeared at E_B = 84.35eV. The fact that the interface component takes a higher E_B value than that for Au bulk indicates electronic charge transfer from Au(001) to NiO(001). Intuitively, the electrons bound to Au are transferred to the above O atom. This charge transfer will be discussed later based on the *ab initio* calculations using VASP.

It is interesting to see the band gap dependent on the thickness of NiO(001) on Au(001). Electron energy loss spectroscopy (EELS) gives information on band gap (*EG*) as the energy loss of the inter-band transition. Figure 6 shows the EELS spectrum observed for 200 eV electron incidence on NiO(10 ML)/Au(10 ML)/Ag(001). The small peak seen around 197.5 eV corresponds to excitation of Au surface plasmon[35,36], which can be approximately expressed by a Gaussian shape. The observed spectrum can be fitted by a Fermi-Dirac distribution coupled with a Gaussian shape, given by

$$f(E) = A_1 + \frac{(A_2 - A_1)}{1 + \exp\{(E - E_0)/\Delta E\}} + \frac{A_0}{\sigma\sqrt{2\pi}} \exp\{-(E - E_P)^2 / 2\sigma^2\} \quad (2)$$

where A_0, A_1, A_2, E_0, ΔE, E_P, and σ are fitting parameters. The tangent of the Fermi edge crosses the background level and the crossing point (denoted as P in a graph) gives the energy loss due to the inter-band transition, namely the band gap *EG* (see Fig. 6). We thus obtained the *EG* values as a function of NiO(001) thickness, which is indicated in Fig. (7). Contrary to the usual quantum size effect, the band gap of NiO(001) decreases with decreasing the thickness from 10 down to 5ML. Such a phenomenon was also reported for α-Al_2O_3 thin layers grown on Ru(0001) substrate [11]. This may be related to the metallic feature of thin NiO(001) stacked on Au(001), which was predicted based on the DFT calculations in spite of small density of states [32].

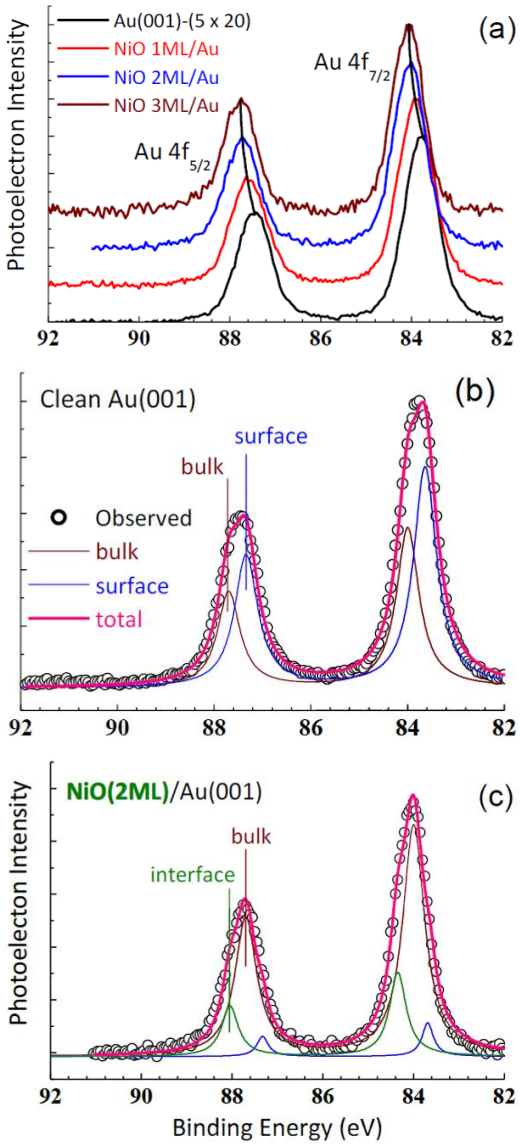

© All Rights Reserved

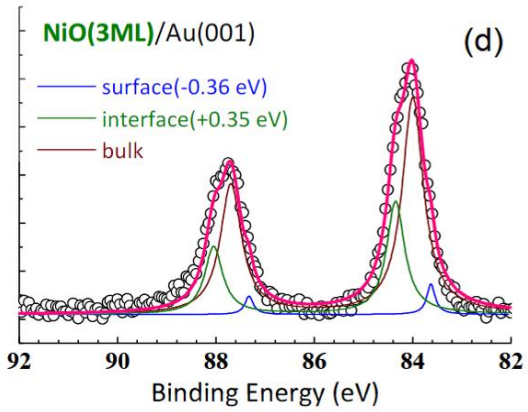

Fig. (5) Au 4f core level spectra observed at 130 eV photon incidence for Au(10ML)/Ag(001) (upper right), NiO(2ML)/Au(10ML) (lower left), NiO(3 ML)/Au(10 ML) (lower right), and total three spectra (upper left). Spectra were decomposed into three components (thin solid curves) coming from surface (lower E_B), bulk, and interface (higher E_B). Thick solid curves are best-fitted total spectra

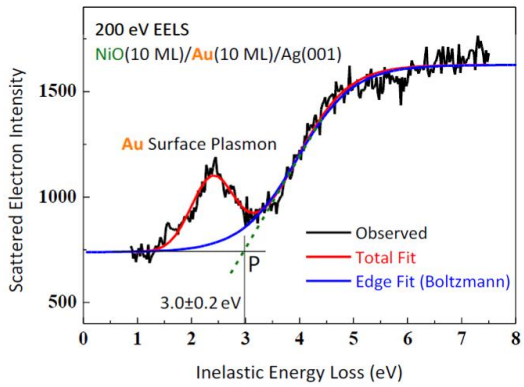

Fig. (6) The EELS spectrum observed for NiO(10 ML)/Au(10 ML)/Ag(001) at 100 eV of electron impact. Observed spectrum was best-fitted by Gaussian coupled with Boltzmann function. Crossing point P between tangent of Fermi edge and background level corresponds to onset of inter-band transition

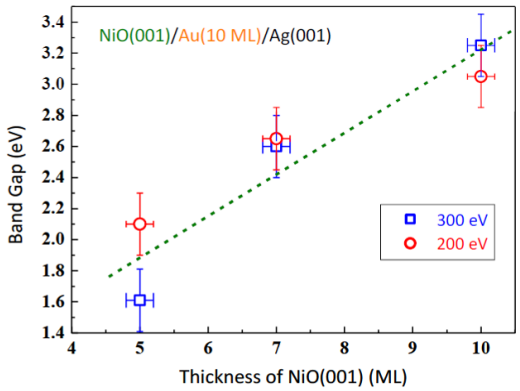

Fig. (7) Band gap values derived from EELS for NiO(001)/Au(001)-10ML/Ag(001) as a function of NiO thickness. Open squares and circles denote the data obtained using 300 and 200 eV electron incidence, respectively

We performed *ab initio* calculations using VASP (Vienna *ab initio* simulation package) [25,26] to explain the atomic structure and electronic properties obtained in the present study. In this calculations, the slab consists of 2 ML of a pseudomorphic NiO(001) and of 5ML of Au(001) with a (2×2) surface unit cell. The bottom Au(001) layer was fixed and the other atoms were free to relax. We used the generalized gradient approximation (GGA) [37] as the exchange-correlation potentials and projector-augmented wave (PAW) method [38] as the basis functions. The cut-off energy for the ρ plane-wave basis was set to 380 eV. For *k* point sampling, we employed the Monkhorst-Pack meshes [39] of 9×9×1 for structure optimization and of 13×13×1 for evaluation of the electronic properties. The partial occupancies for wave functions were estimated by means of Methfessel-Paxton method [40] for the structure optimization and by the tetrahedron method with Blöchl corrections [38] for band structure analysis. The structure optimization calculations were continued until the Hellmann-Feynman force acting on each atom was less than 0.01 eV/Å. In order to consider the insulating nature of NiO, we employed the L(S)DA+U correction realized by Dudarev' approach (local spin density approximation +(U+J) correlation potentials) [27]. The best choice was U = 6.0–6.3 eV and J = 1.0 eV to give a band gap of 3.1 eV and a magnetic moment of 1.67 μ_B (μ_B: Bohr magneton) close to the experimental values of 4.3 eV and 1.7 μ_B.

As the results, the location of the O atoms above Au at the interface is more stable by 0.16 eV/(unit cell) rather than the configuration of Ni above Au, supporting our MEIS result, just like the location of O above Ag for the NiO(001)/Ag(001) interface [12,16]. Concerning the NiO(001)/Au(001) interlayer distance, the present VASP calculations using the (U+J) potentials gave a larger value of 2.60±0.10 Å than the value of 2.30±0.05 Å derived from MEIS analysis. This interlayer distances are affected by choice of exchange–correlation potential (it is commonly known that LDA sometimes overestimates interatomic distances) and (U+J) potential values, which were chosen to give a band gap and magnetic moment closer to the experimental values. This choice may cause the above disagreement.

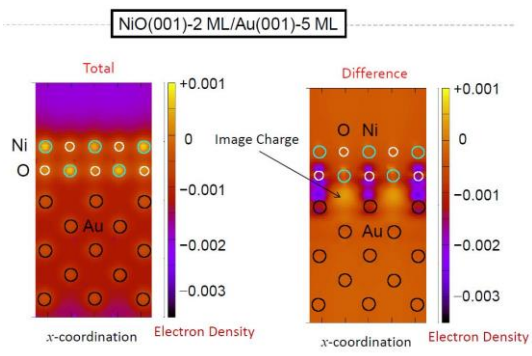

Fig. (8) (Left side panel) Electron charge density distribution

© All Rights Reserved

calculated by VASP for NiO(001)-2ML/Au(001)-5ML. (Right side panel) Difference between the charge density distributions for interacting and non-interacting NiO/Au. Electron condensation is seen beneath the bottom Ni atoms at the interface (image charge)

We then tried to analyze electronic charge transfer occurring between Au substrate and NiO layers. The Bader charge analysis [41] showed very small electronic charge transfer from NiO to Au, ~2×10^{-3} e/Å^2 for 2 ML-NiO stacking and ~7×10^{-4} e/Å^2 for 4 ML-NiO stacking. Note that Au is an electronegative species. This is in contradiction with the higher *EB* shift of the Au 4f interface component. There are other methods to estimate electronic charge transfer such as Mulliken method. In any methods, there still exist ambiguities to some extent. In order to perform more detailed analysis, we evaluated quantitatively the electron charge density distribution for NiO(2 ML)/Au(5 ML), which is indicated in Fig. (8) (left panel). The electron charge density distribution was also calculated for separate non-interacting NiO(001) and Au parts for the same unit cell configuration. Figure (8b) is the difference between the charge density distributions for interacting and non-interacting NiO/Au. Interestingly, an electron rich region emerges beneath the bottom Ni atoms, whereas an electron lack region appears beneath the bottom O atoms, just like the image charge which was predicted by Finnis [42] for metal/ceramics interfaces. The electrons of metal are redistributed to form apparently like a structure of anion above cation and cation on anion at the interface. This situation means that the electrons of the top Au at the interface move to the region below the bottom Ni to form the image charge distribution, which may cause the higher E_B shift of the Au 4f core line. Indeed, no Au 4f core level shift was observed for NiO(111)/Au(111) for NiO thickness from 1 to 3 ML (not shown here). This is probably due to pure Ni/Au interface which does not contain O atoms in that system. The image charge may also lead to band gap narrowing, which has been studied mainly from theoretical view point [43,44]. Unfortunately, no clear explanation has been still given. Finally, it is pointed again that the metallic feature observed for 1-3 ML NiO(001)/Au(001) is intimately related to the band gap narrowing probably in terms of the image charge.

4. Conclusions

We first revealed by MEIS that the O atoms were located above Au atoms at the NiO(001)/Au(001) interface. This was supported by the *ab initio* calculations using VASP. The interlayer distance of 2.30±0.05Å derived from MEIS is comparable with that for NiO(001)/Ag(001), but significantly smaller than that (2.6±0.1Å) predicted by VASP. This disagreement is due to the choice of (U+J) potentials, which were taken to give a magnetic moment and large band gap close to those for bulk NiO. Concerning the electronic properties of the NiO/Au interface, we observed metallic features for NiO(001)/Au(001) for NiO thickness up to 3 ML. We also observed the interface component for Au 4f core level, which shifted by 0.35 eV to higher E_B side compared with that for bulk Au. Despite that, the *ab initio* calculations using VASP demonstrated no significant charge transfer, which was evaluated quantitatively by the Bader charge analysis.

References

[1] A. Ohtomo and H.Y. Hwang, Nature 427 (2004) 423.
[2] A.F. Santaner-Syro, O. Copie, T. Kondo, F. Fortuna, S. Pailhès, R. Weht, X.G. Qiu, F. Bertran, A. Nicolaou, A. Taleb-Ibrahimi, P. Le Fèvre, G. Herranz, M. Bibes, N. Reyren, Y. Apertet, P. Lecoeur, A. Barthélémy, M.J. Rozenberg, Nature 469 (2011) 189.
[3] M. D'Angelo, R. Yukawa, K. Ozawa, S. Yamamoto, T. Hirahara, S. Hasegawa, M.G. Silly, F. Sirotti, and I. Matsuda, Phys. Rev. Lett. 108 (2012) 116802.
[4] J.G. Wang and B. Hammer, Phys. Rev. Lett. 97 (2006) 136107.
[5] H. Shi, M. Kohyama, S. Tanaka, and S. Takeda, Phys. Rev. B 80 (2009) 155413.
[6] K. Mitsuhara, M. Tagami, T. Matsuda, A. Visikovskiy, M. Takizawa, and Y. Kido, J. Chem. Phys. 136 (2012) 124303.
[7] M. Haruta, Chem. Record 3 (2003) 75.
[8] M. Haruta, N. Yamada, T. Kobayashi, and S. Iijima, J. Catal. 115 (1989) 301. [9] G.A. Sawatzky and J.W. Allen, Phys. Rev. Lett. 53 (1984) 2339.
[10] O. Miura and T. Fujiwara, Phys. Rev. B 77 (2008) 195124.
[11] Y. Murata, K. Nagata, H. Fujimoto, T. Sakurai, M. Okada, and Y. Ebe, J. Phys. Soc. Jpn. 70 (2001) 793.
[12] C. Lamberti, E. Groppo, C. Prestipino, S. Casassa, A.M. Ferrari, C. Pisani, C. Giovanardi, P. Luches, S. Valeri, and F. Boscherini, Phys. Rev. Lett. 91 (2003) 046101.
[13] D. Spanke, V. Solinus, D. Knabben, F.U. Hillebrecht, F. Ciccacci, L. Gregoratti, and M. Marsi, Phys. Rev. B 58 (1998) 5201.
[14] C. Lamberti, Surf. Sci. Reports 53 (2004) 1.
[15] S. Casassa, A.M. Ferrari, M. Busso, and C. Pisani, J. Phys. Chem. B 106 (2002) 12978.
[16] M. Cafio, B. Cortigiani, G. Rovida, A. Atrei, C. Giovanardi, A.di Bona, and S. Valeri, Surf. Sci. 531 (2003) 368.
[17] C. Giovanardi, A. di Bona, and S. Valeri, Phys. Rev. B 69 (2004) 075418.
[18] E. Groppo, C. Prestipino, C. Lamberti, R. Carboni, F. Boscherini, P. Luches, S. Valeri, and S. D'Addato, Phys. Rev. B 70 (2004) 165408.

© All Rights Reserved

[19] R. de Masi, D. Reinicke, F. Müller, P. Steiner, and S. Hüfner, Surf. Sci. 515 (2002) 523.
[20] T. Okazawa, M. Fujiwara, T. Nishimura, T. Akita, M. Kohyama and Y. Kido, Surf. Sci. 600 (2006) 1331.
[21] S. Benedetti, P. Torelli, P. Luches, A. Rota, and S. Valeri, Surf. Sci. 600 (2006) 4251.
[22] A. Barbier, C. Mocuta, H. Kuhlenbeck, K.F. Peters, B. Richter, and G. Renaud, Phys. Rev. Lett. 84 (2000) 2897.
[23] T. Okazawa, T. Nishizawa, T. Nishimura and Y. Kido, Phys. Rev. B 75 (2007) 033413.
[24] Y. Kido, H. Namba, T. Nishimura, A. Ikeda, Y. Yan and A. Yagishita, Nucl. Instrum. Methods Phys. Res. B 136-138 (1998) 798.
[25] G. Kresse and J. Hafner, Phys. Rev. B 47 (1993) 558.
[26] G. Kresse and J. Furthmüller, Phys. Rev. B 54 (1996) 11169.
[27] S.L. Dudarev, G.A. Savrasov, C.H. Hamphreys, and A.P. Sutton, Phys. Rev. B 57 (1998) 1505.
[28] D.M. Kolb and J. Schneider, Electrochem. Acta 31, 929 (1986) 929.
[29] T. Okazawa, Y. Yagi and Y. Kido, Phys. Rev. B 67 (2003) 195406.
[30] A. Rota, S. Altieri, and S. Valeri, Phys. Rev. B 79 (2009) 161401.
[31] S. Hüfner, Photoelectron Spectroscopy (Springer, 2003, Berlin).
[32] I.O. Thomas and A. Fortunelli, Eur. Phys. J. B 75 (2010) 5.
[33] T.C. Hsieh, A.P. Shapiro, and T.-C. Chiang, Phys. Rev. B 31 (1985) 2541.
[34] A. Tanaka, Y. Takeda, T. Nagasawa, H. Sasaki, Y. Kuriyama, S. Suzuki, and S. Sato, Surf. Sci. 532 (2003) 281.
[35] H.A.E. Hagelin-Weaver, J.F. Weaver, G.B. Hoflund, and G.N. Salaita, J. Alloys Compounds 393 (2005) 93.
[36] A. Politano and G. Chiarello, Gold Bulletin 42 (2009) 195.
[37] J.P. Perdew, K. Burke, and M. Erzerhof, Phys. Rev. Lett. 77 (1996) 3865.
[38] P.E. Blöchl, Phys. Rev. B 50 (1994) 17953.
[39] H.J. Monkhorst and J.D. Pack, Phys. Rev. B 13 (1976) 5188.
[40] M. Methfessel and A.T. Paxton, Phys. Rev. B 40 (1989) 3616.
[41] R.F.W. Bader, Atoms in Molecules -A quantum theory (Oxford University Press, New York, 1990).
[42] M.W. Finnis, J. Phys. Condens. Mat. 8 (1996) 5811.
[43] J.P.A. Charlesworth, R.W. Godby, and R.J. Needs, Phys. Rev. Lett. 70 (1993) 1685.
[44] R. Arita, Y. Tanida, K. Kuroki, and H. Aoki, Phys. Rev. B 64 (2001) 245112.
[45] O.A. Hamadi, K.Z. Yahiya and O.N.S. Jassim, J. Semicond. Sci. Technol., 5(3) 182-186 (2005).
[46] K.S. Khashan and O.A. Hamadi, Eng. Technol. J., 25(2) 168-175 (2007).
[47] O.A. Hamadi, Iraqi J. Appl. Phys. Lett., 1(2) 3-8 (2008).
[48] O.A. Hamadi, B.A.M. Bader and A.K. Yousif, Eng. Technol. J., 26(8) 995-1001 (2008).
[49] A.A. Hadi and O.A. Hamadi, Iraqi J. Appl. Phys. Lett., 1(2) 23-26 (2008).
[50] A.K. Yousif and O.A. Hamadi, Bulg. J. Phys., 35(3) 191-197 (2008).
[51] O.A. Hamadi, N.J. Shakir, F.H. Hussain, Bulg. J. Phys., 37(4), 223-231 (2010).
[52] O.A. Hamadi, Iraqi J. Appl. Phys. Lett., 3(1) 23-26 (2010).
[53] O.A. Hammadi and N.E. Naji, Iraqi J. Appl. Phys., 10(2) 27-31 (2014).
[54] O.A. Hammadi, W.N. Raja, M.A. Saleh and
[55] W.A. Altun, Iraqi J. Appl. Phys., 12(3), 35-42 (2016).
[56] O.A. Hammadi, W.N. Raja, M.A. Saleh and W.A. Altun, Iraqi J. Appl. Phys., 12(4), 19-28 (2016).
[57] O.A. Hammadi, J. Optoelectron. Phot., 7(5), 21 (2016).
[58] O.A. Hammadi, J. Laser Micro/Nanoeng., 11(6), 151 (2016).
[59] O.A. Hammadi, J. Biomed. Nanotechnol., 12(8), (2016).
[60] O.A. Hamadi, Iraqi J. Appl. Phys., 12(2) 9-13 (2016).
[61] O.A. Hammadi, Photonic Sensors, 6(4) 345-350 (2016). DOI: 10.1007/s13320-016-0338-4
[62] O.A. Hammadi and N.E. Naji, Photonic Sensors, 8(1) 43-47 (2018).

© All Rights Reserved